BOUNDARY ELEMENT APPROACH TO THE DYNAMIC STIFFNESS FUNCTIONS OF CIRCULAR FOUNDATIONS

E. ALARCON AND J. J. CANO

AND

J. DOMINGUEZ

INTRODUCTION

In the past twenty years numerous investigations which deal with the computation of dynamic stiffness (also called impedance) matrices of massless rigid foundations with different shapes have been reported. Taking advantage of the simplifications derived from axial symmetry, circular and cylindrical foundations have been studied in many cases. Analytical solutions for stiffness functions of circular foundations on a uniform half-space were presented for horizontal and rocking motions by Veletsos and Wei[1] and for vertical and torsional motions by Luco and Westman.[2]

The development of absorbing boundaries permitted the use of the finite element method to study the dynamic response of axisymmetric foundations on soils that consist of one or several layers based on a rigid rock.[3-5]

An alternative approach to the dynamic analysis of rigid foundations is the use of boundary integral equations which allow for the modelling of many different geometries and soil profiles. Both the direct and the indirect integral equation formulations have been used in dynamic soil–structure interaction problems.[6-8] Dynamic stiffness functions of rigid circular foundations on uniform or layered soils have been computed by Apsel[9] and Apsel and Luco[7] using the indirect formulation in combination with Green's function of a ring load in a uniform or layered half-space, derived by the same authors.[9-11] This Green's function is written in terms of integral forms

that include products of two Bessel functions. Owing to that, it has to be evaluated segmentally and its computation becomes rather involved. An auxiliar boundary where the unknown sources are located has to be defined.[7,9,12]

The boundary element method, based on the direct integral equation formulation, has been used to compute dynamic stiffness functions of rectangular[6] and strip foundations in the frequency domain[13,14] as well as in the time domain.[15] In the present paper the boundary element method is formulated for time harmonic axisymmetric problems using the full-space point load fundamental solution. The approach is applied to the computation of the dynamic stiffness functions of rigid circular foundations on layered viscoelastic soils.

The formulation of the BEM for axisymmetric elastostatic problems was presented by Kermanidis[16] and Cruse *et al.*[17] They used the ring load fundamental solution. However, a closed form expression for the ring load does not exist in elastodynamics[18] and when the same formulation is followed the computations become involved because of the difficulties in the evaluation of the fundamental solution at each integration point. On the contrary, the point load fundamental solution is simple and may be integrated numerically along the azimuthal co-ordinate without any particular difficulty.

As an example of the range of sites to which the proposed approach can be applied, three different sites are considered; a uniform half-space, a soil layer on a half-space, and a soil consisting of four horizontal layers and a compliant half-space. The numerical results computed by the proposed approach are compared with results obtained by different procedures.

BOUNDARY ELEMENT FORMULATION FOR ELASTODYNAMIC AXISYMMETRIC PROBLEMS

Following the idea of Chapel,[19] the full-space point load fundamental solution is used to solve time harmonic axisymmetric problems. The axisymmetric representation of the geometry and field variables is maintained. The boundary of the generating surface of the body is discretized into line elements and the point load collocated at each node. The fundamental solution, in terms of cylindrical co-ordinates, is integrated along the boundary elements of the generating surface and along the azimuthal co-ordinate.

The basic BEM equation for zero body forces can be written in Cartesian co-ordinates as usual:

$$\mathbf{C}^i\mathbf{u}^i + \int_\Gamma \mathbf{T}\mathbf{u}\,d\Gamma = \int_\Gamma \mathbf{U}\mathbf{t}\,d\Gamma \tag{1}$$

where $\mathbf{u}$ and $\mathbf{t}$ stand for the displacements and traction vectors, respectively; $\mathbf{U}$ and $\mathbf{T}$ are, respectively, the matrices representing displacements and tractions produced by the point load applied at point i and $\mathbf{C}$ is the independent coefficient matrix such that $C_{kl} = (1/2)\delta_{kl}$ when the surface is smooth at the point i.

The relation between Cartesian and cylindrical co-ordinates may be written for vectors $\mathbf{u}$ and $\mathbf{t}$ at a certain point j as

$$\mathbf{u} = \mathbf{Q}\mathbf{u}_c \qquad \mathbf{t} = \mathbf{Q}\mathbf{t}_c \tag{2}$$

where the subindex 'c' stands for cylindrical (Figure 1) and the transformation matrix is

$$\mathbf{Q} = \begin{bmatrix} \cos\vartheta & -\sin\vartheta & 0 \\ \sin\vartheta & \cos\vartheta & 0 \\ 0 & 0 & 1 \end{bmatrix} \tag{3}$$

By substitution of equation (2) into equation (1) and premultiplying by $\mathbf{Q}^{i,\mathrm{T}}$ the following equation is obtained:

$$\mathbf{Q}^{i,\mathrm{T}}\,\mathbf{C}^{i}\,\mathbf{Q}^{i}\,\mathbf{u}_{\mathrm{c}}^{i} + \int_{\Gamma}(\mathbf{Q}^{i,\mathrm{T}}\,\mathbf{T}\mathbf{Q})\,\mathbf{u}_{\mathrm{c}}\,\mathrm{d}\Gamma = \int_{\Gamma}(\mathbf{Q}^{i,\mathrm{T}}\,\mathbf{U}\mathbf{Q})\,\mathbf{t}_{\mathrm{c}}\,\mathrm{d}\Gamma \tag{4}$$

where $\mathbf{Q}^{i}$ is the transformation matrix for the collocation point *i*. Equation (4) can now be written as

$$\mathbf{C}_{\mathrm{c}}^{i}\,\mathbf{u}_{\mathrm{c}}^{i} + \int_{\Gamma}\mathbf{T}_{\mathrm{c}}\,\mathbf{u}_{\mathrm{c}}\,\mathrm{d}\Gamma = \int_{\Gamma}\mathbf{U}_{\mathrm{c}}\,\mathbf{t}_{\mathrm{c}}\,\mathrm{d}\Gamma \tag{5}$$

which is the same as equation (1) written in cylindrical co-ordinates.

The ϑ co-ordinate of the collocation point *i* is fixed during the integration process and can be set equal to any desired value; for instance $\vartheta^{i} = 0$. In such a case

$$\mathbf{T}_{\mathrm{c}} = \mathbf{Q}^{i,\mathrm{T}}\,\mathbf{T}\mathbf{Q} = \begin{bmatrix} T_{11}\cos\vartheta + T_{12}\sin\vartheta & -T_{11}\sin\vartheta + T_{12}\cos\vartheta & T_{13} \\ T_{21}\cos\vartheta + T_{22}\sin\vartheta & -T_{21}\sin\vartheta + T_{22}\cos\vartheta & T_{23} \\ T_{31}\cos\vartheta + T_{32}\sin\vartheta & -T_{31}\sin\vartheta + T_{32}\cos\vartheta & T_{33} \end{bmatrix} \tag{6}$$

where the terms T_{kl} are the well-known Cartesian co-ordinate components of the tractions in the *l* direction at the integration point, due to a unit point load in the *k* direction at the point *i*. The same equation can be written for $\mathbf{U}_{\mathrm{c}}$.

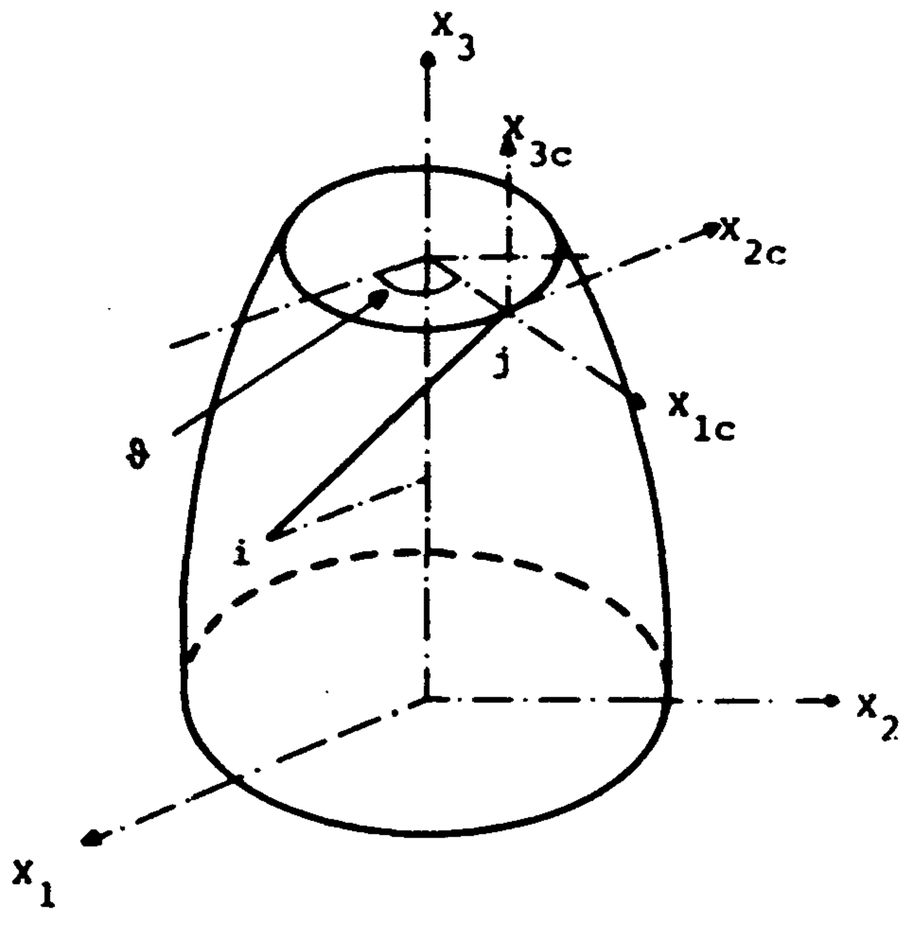

Figure 1. Description of co-ordinate systems

When a circular foundation under vertical or torsional motion is considered, the field variables are axisymmetric. Assuming that the boundary is smooth at i, equation (5) becomes

$$\frac{1}{2}\begin{bmatrix} u_\rho^i \\ u_\vartheta^i \\ u_z^i \end{bmatrix} + 2\int_{\Gamma^*} \rho \left[\int_0^\pi \begin{bmatrix} T_{11}\mathrm{c}\vartheta + T_{12}\mathrm{s}\vartheta & 0 & T_{13} \\ 0 & -T_{21}\mathrm{s}\vartheta + T_{22}\mathrm{c}\vartheta & 0 \\ T_{31}\mathrm{c}\vartheta + T_{32}\mathrm{s}\vartheta & 0 & T_{33} \end{bmatrix} \mathrm{d}\vartheta \right] \begin{bmatrix} u_\rho \\ u_\vartheta \\ u_z \end{bmatrix} \mathrm{d}\Gamma^*$$

$$= 2\int_{\Gamma^*} \rho \left[\int_0^\pi \begin{bmatrix} U_{11}\mathrm{c}\vartheta + U_{12}\mathrm{s}\vartheta & 0 & U_{13} \\ 0 & -U_{21}\mathrm{s}\vartheta + U_{22}\mathrm{c}\vartheta & 0 \\ U_{31}\mathrm{c}\vartheta + U_{32}\mathrm{s}\vartheta & 0 & U_{33} \end{bmatrix} \mathrm{d}\vartheta \right] \begin{bmatrix} t_\rho \\ t_\vartheta \\ t_z \end{bmatrix} \mathrm{d}\Gamma^* \qquad (7)$$

where Γ^* is the boundary of the generating surface (Figure 2), s and c stand for sin and cos, respectively and a zero has been placed for the skewsymmetric terms, where the integrals around the azimuthal axis are null. It should be mentioned that the torsional and vertical-radial motions are uncoupled in equation (7) and that the kernels to be integrated along ϑ are known functions.

When a circular foundation is under horizontal motion along X_1 or rocking around X_2, the field variables are of the form (Figure 3)

$$\begin{aligned} u_\rho &= u_{1\rho}\cos\vartheta \; ; \qquad t_\rho = t_{1\rho}\cos\vartheta \\ u_\vartheta &= -u_{1\vartheta}\sin\vartheta \; ; \qquad t_\vartheta = -t_{1\vartheta}\sin\vartheta \\ u_z &= u_{1z}\cos\vartheta \; ; \qquad t_z = t_{1z}\cos\vartheta \end{aligned} \qquad (8)$$

where $u_{1\rho}$, $u_{1\varphi}$, u_{1z}, $t_{1\rho}$, $t_{1\varphi}$ and t_{1z} are independent of ϑ. Instead of equation (7) the following

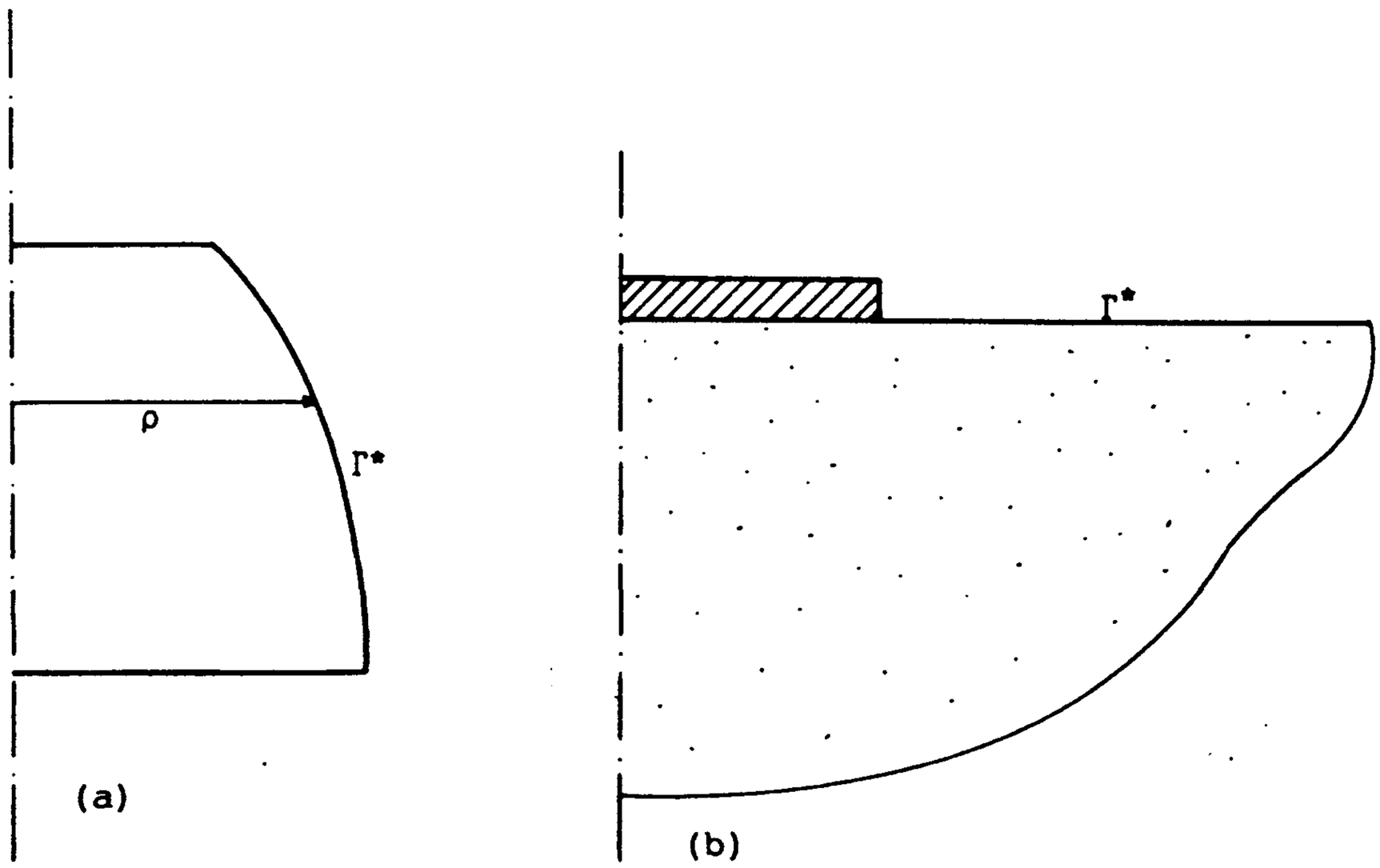

Figure 2. Generating surface of an axisymmetric domain: (a) general problem; (b) surface foundation on a half-space

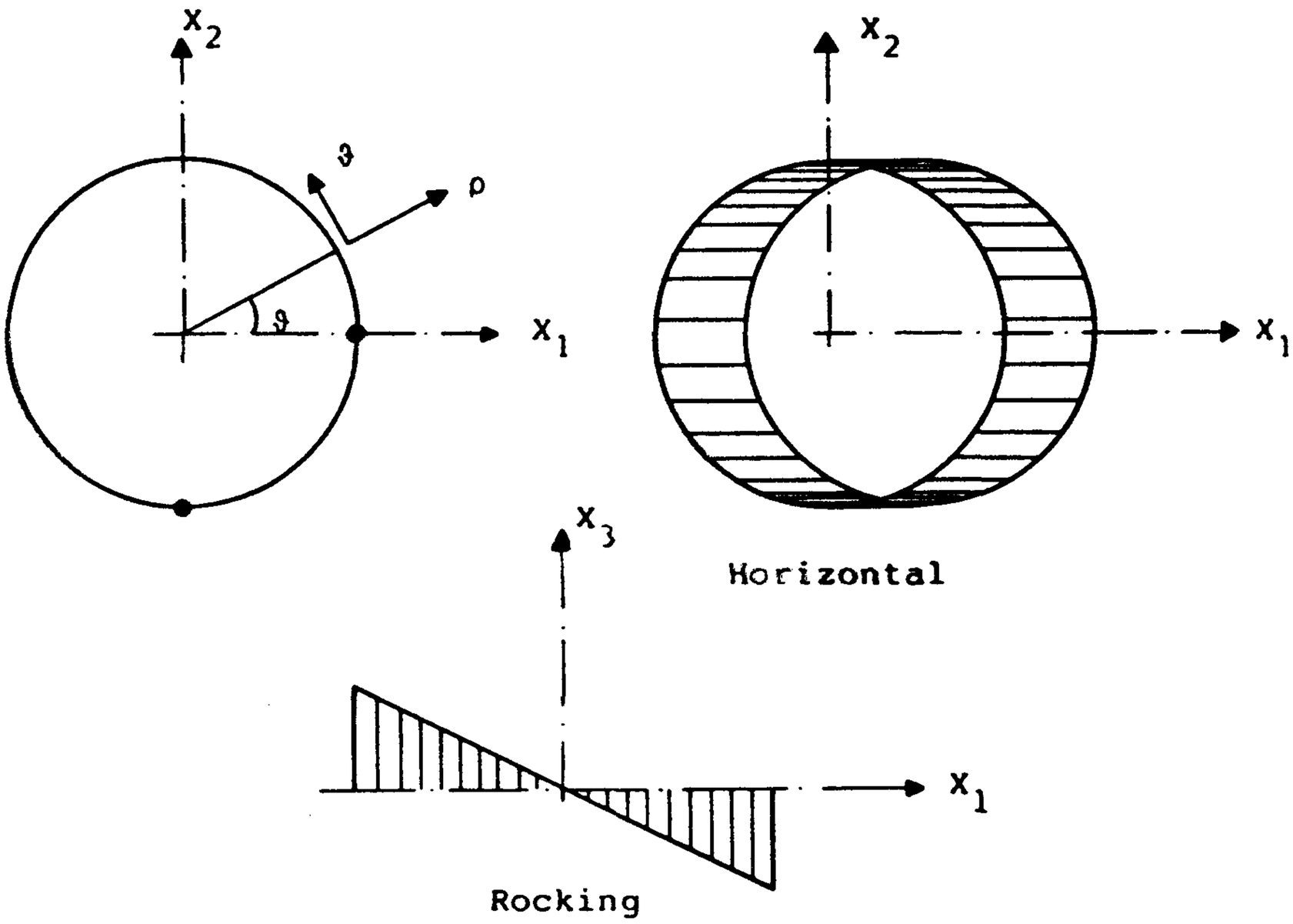

Figure 3. Horizontal and rocking displacement

equation is obtained:

$$\frac{1}{2}\begin{bmatrix} u^i_{1\rho} \\ 0 \\ u^i_{1z} \end{bmatrix} + 2\int_{\Gamma^*}\rho\left[\int_0^{\pi}\begin{bmatrix} T_{11}c^2\vartheta + T_{12}s\vartheta c\vartheta & T_{11}s^2\vartheta - T_{12}s\vartheta c\vartheta & T_{13}c\vartheta \\ 0 & 0 & 0 \\ T_{31}c^2\vartheta + T_{32}s\vartheta c\vartheta & T_{31}s^2\vartheta - T_{32}s\vartheta c\vartheta & T_{33}c\vartheta \end{bmatrix} d\vartheta\right]\begin{bmatrix} u_{1\rho} \\ u_{1\vartheta} \\ u_{1z} \end{bmatrix} d\Gamma^*$$

$$= 2\int_{\Gamma^*}\rho\left[\int_0^{\pi}\begin{bmatrix} U_{11}c^2\vartheta + U_{12}s\vartheta c\vartheta & U_{11}s^2\vartheta - U_{12}s\vartheta c\vartheta & U_{13}c\vartheta \\ 0 & 0 & 0 \\ U_{31}c^2\vartheta + U_{32}s\vartheta c\vartheta & U_{31}s^2\vartheta - U_{32}s\vartheta c\vartheta & U_{33}c\vartheta \end{bmatrix} d\vartheta\right]\begin{bmatrix} t_{1\rho} \\ t_{1\vartheta} \\ t_{1z} \end{bmatrix} d\Gamma^* \quad (9)$$

Equation (9) can be used to represent the radial and vertical displacements but not the azimuthal displacement for which an identity would be obtained. The amplitude of a function such as $u_\vartheta = u_{1\vartheta}\sin\vartheta$ cannot be computed with a collocation point where the function is zero. Because of this, a different collocation point where the shape function $-\sin\vartheta^i$ has a unit amplitude ($\vartheta^i = -\pi/2$) is selected for the azimuthal equation:

$$\mathbf{T}^0_c = \mathbf{Q}^{i,\mathrm{T}}\mathbf{T}\mathbf{Q} = \begin{bmatrix} -T^0_{21}c\vartheta - T^0_{22}s\vartheta & T^0_{21}s\vartheta - T^0_{22}c\vartheta & -T^0_{23} \\ T^0_{11}c\vartheta + T^0_{12}s\vartheta & -T^0_{11}s\vartheta + T^0_{12}c\vartheta & T^0_{13} \\ T^0_{31}c\vartheta + T^0_{32}s\vartheta & -T^0_{31}s\vartheta + T^0_{32}c\vartheta & T^0_{33} \end{bmatrix} \quad (10)$$

where the superindex '0' indicates that the collocation point is at $\vartheta^i = -\pi/2$. The equation that represents the three components is

$$\frac{1}{2}\begin{bmatrix} u^i_{1\rho} \\ u^i_{1\vartheta} \\ u^i_{1z} \end{bmatrix} + 2\int_{\Gamma^*} \rho \left[\begin{array}{c|c|c} \int_0^{\pi} (T_{11}c^2\vartheta + T_{12}s\vartheta c\vartheta)\,d\vartheta & \int_0^{\pi} (T_{11}s^2\vartheta - T_{12}s\vartheta c\vartheta)\,d\vartheta & \int_0^{\pi} (T_{13}c\vartheta)\,d\vartheta \\ \hline \int_{-\pi/2}^{\pi/2} (T^0_{11}c^2\vartheta + T^0_{12}s\vartheta c\vartheta)\,d\vartheta & \int_{-\pi/2}^{\pi/2} (T^0_{11}s^2\vartheta - T^0_{12}s\vartheta c\vartheta)\,d\vartheta & \int_{-\pi/2}^{\pi/2} (T^0_{13}c\vartheta)\,d\vartheta \\ \hline \int_0^{\pi} (T_{31}c^2\vartheta + T_{32}s\vartheta c\vartheta)\,d\vartheta & \int_0^{\pi} (T_{31}s^2\vartheta - T_{32}s\vartheta c\vartheta)\,d\vartheta & \int_0^{\pi} (T_{33}c\vartheta)\,d\vartheta \end{array}\right] \begin{bmatrix} u_{1\rho} \\ u_{1\vartheta} \\ u_{1z} \end{bmatrix} d\Gamma^*$$

$$= 2\int_{\Gamma^*} \rho \left[\begin{array}{c|c|c} \int_0^{\pi} (U_{11}c^2\vartheta + U_{12}s\vartheta c\vartheta)\,d\vartheta & \int_0^{\pi} (U_{11}s^2\vartheta - U_{12}s\vartheta c\vartheta)\,d\vartheta & \int_0^{\pi} (U_{13}c\vartheta)\,d\vartheta \\ \hline \int_{-\pi/2}^{\pi/2} (U^0_{11}c^2\vartheta + U^0_{12}s\vartheta c\vartheta)\,d\vartheta & \int_{-\pi/2}^{\pi/2} (U^0_{11}s^2\vartheta - U^0_{12}s\vartheta c\vartheta)\,d\vartheta & \int_{-\pi/2}^{\pi/2} (U^0_{13}c\vartheta)\,d\vartheta \\ \hline \int_0^{\pi} (U_{31}c^2\vartheta + U_{32}s\vartheta c\vartheta)\,d\vartheta & \int_0^{\pi} (U_{31}s^2\vartheta - U_{32}s\vartheta c\vartheta)\,d\vartheta & \int_0^{\pi} (U_{33}c\vartheta)\,d\vartheta \end{array}\right] \begin{bmatrix} t_{1\rho} \\ t_{1\vartheta} \\ t_{1z} \end{bmatrix} d\Gamma^* \qquad (11)$$

In general, non-axisymmetric boundary conditions can be analyzed using a plane model by representing the field variables by a Fourier series along the azimuthal co-ordinate. The series is of the form

$$u_\rho = \sum_{n=0}^{\infty} (u^s_{n\rho}\cos n\vartheta + u^a_{n\rho}\sin n\vartheta)$$

$$u_\vartheta = \sum_{n=0}^{\infty} (-u^s_{n\vartheta}\sin n\vartheta + u^a_{n\vartheta}\cos n\vartheta) \qquad (12)$$

$$u_z = \sum_{n=0}^{\infty} (u^s_{nz}\cos n\vartheta + u^a_{nz}\sin n\vartheta)$$

where 's' indicates symmetric terms and 'a' antisymmetric ones. The Fourier modes are uncoupled and a boundary equation may be written for the amplitude of the symmetric and the antisymmetric parts of each mode. The equations for the amplitude of the terms of the form $\sin n\vartheta$ are obtained using a point at $\vartheta^i = -\pi/2n$ as the collocation point.

The integrals in equations (7) and (11) are evaluated numerically except when working in the element that contains the collocation point. In the next section, an integration procedure for constant elements contained in planes x_3 = constant is presented. This kind of element is the only one needed for the analysis of circular foundations on uniform or layered soils.

INTEGRATION OVER THE BOUNDARY ELEMENTS

Constant boundary elements with one node per element are considered (Figure 4). The boundaries of the circular foundation problems analyzed are perpendicular to the X_3-axis and the line boundary co-ordinate Γ^* coincides with the radial cylindrical co-ordinate ρ. Equations (7) and (11) can be written after discretization as

$$\left(\frac{1}{4}\right)\mathbf{u}^i_c + \sum_{j=1}^{N} \left\{ \int_{\rho_j} \rho \left[\int_{\vartheta} \mathbf{T}_c\,d\vartheta \right] d\rho \right\} \mathbf{u}^j_c = \sum_{j=1}^{N} \left\{ \int_{\rho_j} \rho \left[\int_{\vartheta} \mathbf{U}_c\,d\vartheta \right] d\rho \right\} \mathbf{t}^j_c \qquad (13)$$

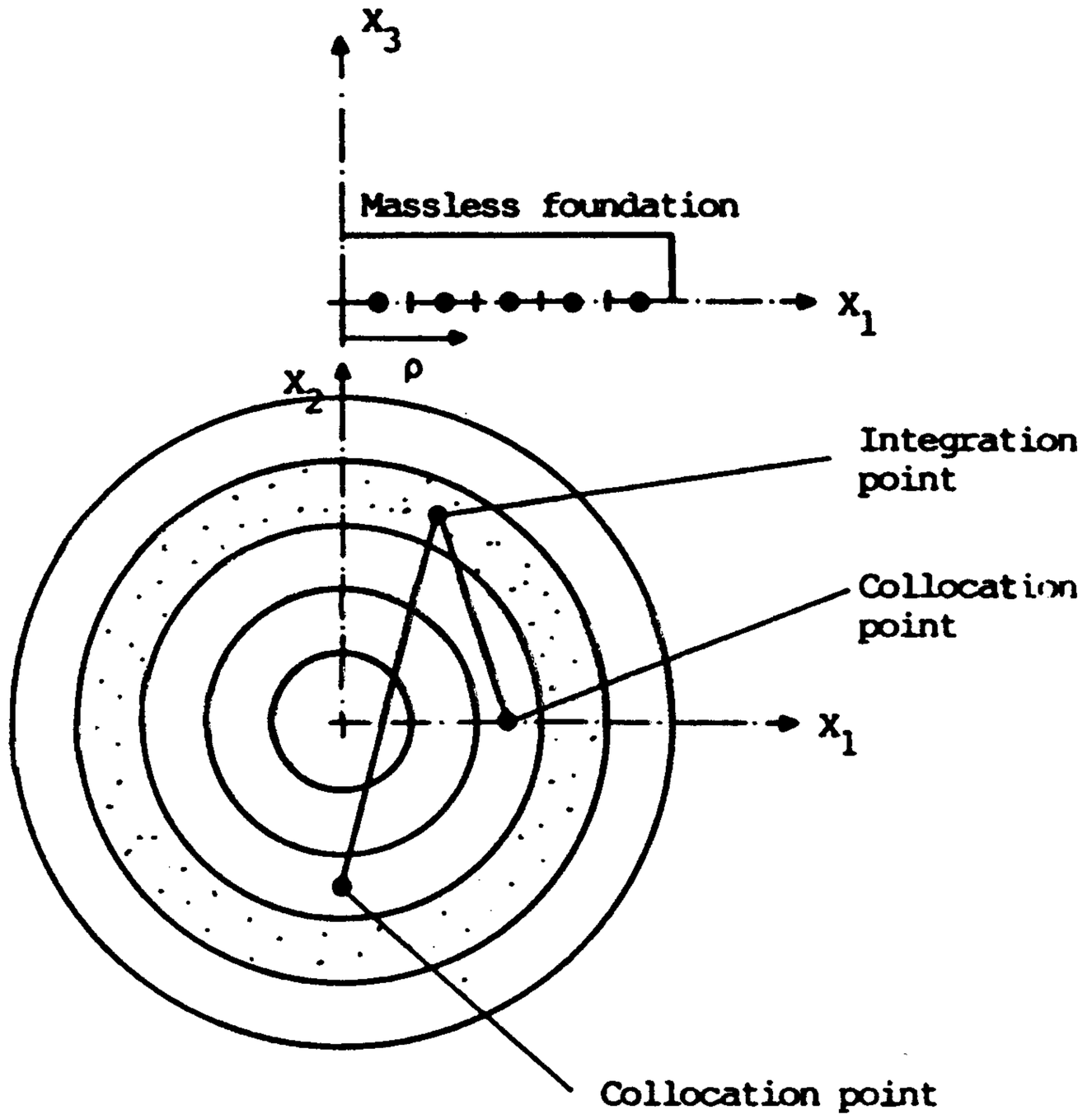

Figure 4. Boundary element discretization

where N is the number of boundary elements, ρ_j indicates the segment that forms the element j, and $\mathbf{T}_e$ and $\mathbf{U}_e$ stand for the matrices in equations (7) or (11). The double integrals extend over one half of the circular crowns represented by the line elements (Figure 4). The collocation point for equation (13) can be either at $\vartheta^i = 0$ or at $\vartheta^i = -\pi/2$ and for each term the integration domain is either the element to which the collocation point belongs ($i = j$) or a different one ($i \neq j$). The latter case is analysed first. The integrals are done numerically using a Gaussian quadrature formula after a special co-ordinate transformation. The integration domain is shown in Figures 5(a) and 5(b), the latter being for the case when the collocation point is at $\vartheta^i = -\pi/2$.

In order to apply the Gaussian quadrature the domain is transformed into a square in the dimensionless co-ordinates ($-1 \leq \xi \leq 1$, $-1 \leq \eta \leq 1$). The radius ρ is transformed into η by

$$\rho = \frac{1}{2}[(R_1 + R_2) + \eta(R_2 - R_1)]$$
$$\mathrm{d}\rho = \frac{1}{2}(R_2 - R_1)\,\mathrm{d}\eta \tag{14}$$

A linear transformation of the same kind was tested for the co-ordinate ϑ; however, the accuracy of the computed values of the integrals was poor even when a large number of integration points was used. The accuracy was improved, and satisfactory results were obtained, by using a quadratic transformation formula that increases the number of integration points in the vicinity of the X_1-axis or the X_2-axis in the cases of Figures 5(a) or 5(b), respectively.[20] The following

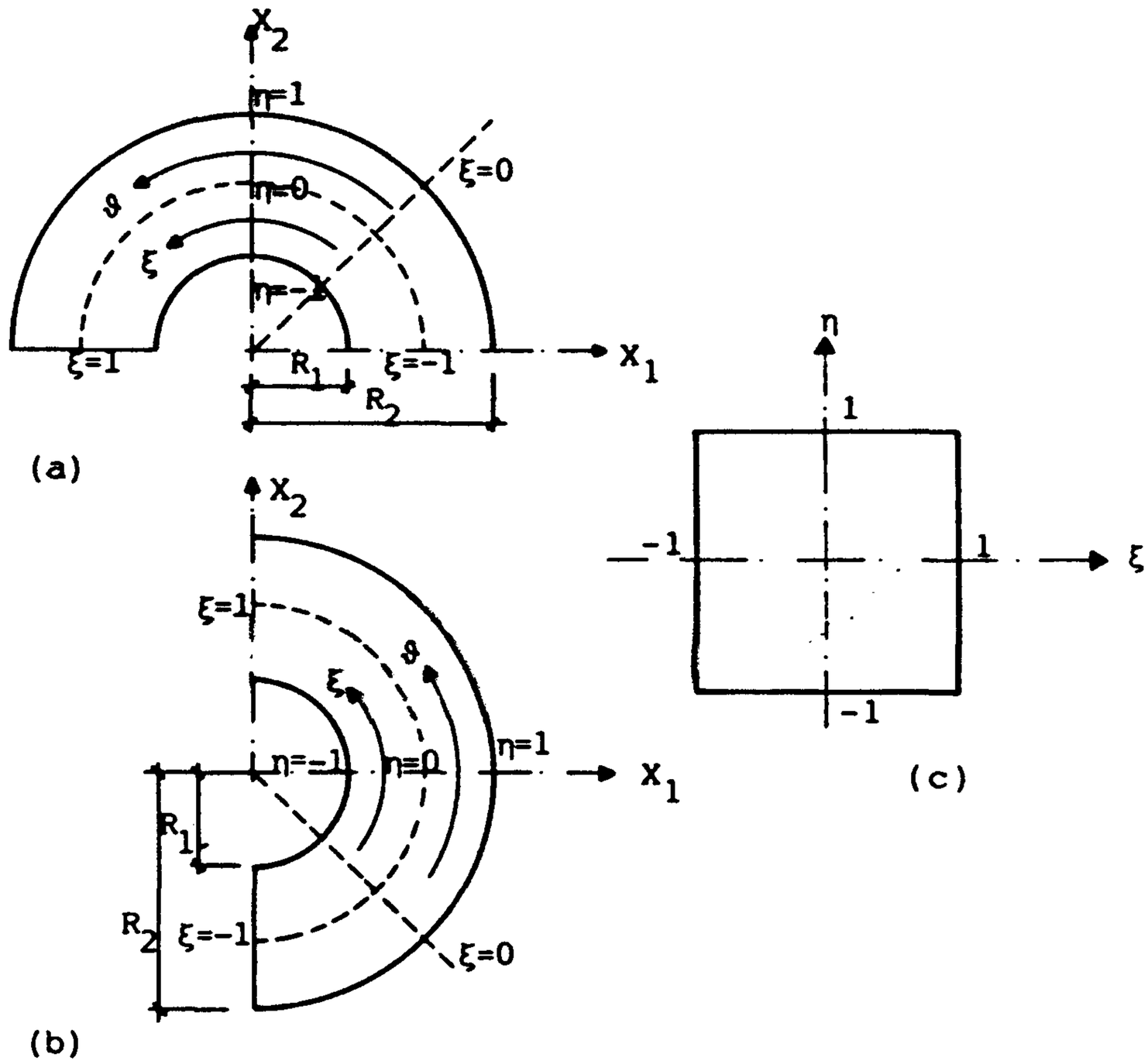

Figure 5. Integration domains and coordinates when the collocation point is outside the integration domain: (a) $\vartheta^i = 0$, (b) $\vartheta^i = -\pi/2$

parabolic transformation has been applied;

$$\left.\begin{aligned} \vartheta &= \frac{\pi}{4}(1+\xi)^2 \\ \mathrm{d}\vartheta &= \frac{\pi}{2}(1+\xi)\,\mathrm{d}\xi \end{aligned}\right\} \tag{15}$$

when the collocation point is at $\vartheta^i = 0$ (Figure 5(a)) and

$$\left.\begin{aligned} \vartheta &= \frac{\pi}{4}(-1+2\xi+\xi^2) \\ \mathrm{d}\vartheta &= \frac{\pi}{2}(1+\xi)\,\mathrm{d}\xi \end{aligned}\right\} \tag{16}$$

when the collocation point is at $\vartheta^i = -\pi/2$ (Figure 5(b)). In this way one half of the total number of integration points are located in the quarter of the domain closer to the collocation point.

The number of quadrature points is two for the radial co-ordinate and twenty for the azimuthal co-ordinate. Thus, the integrals in equation (13) become

$$\mathbf{H}^{*ij} = \int_{\rho_j} \rho \left[\int_{\vartheta} \mathbf{T}_c \,\mathrm{d}\vartheta \right] \mathrm{d}\rho = \sum_{m=1}^{2} \sum_{n=1}^{20} (\pi/4)\,[(R_1 + R_2) + \eta_m (R_2 - R_1)]\,\mathbf{T}_c(\xi_n, \eta_m)[R_2 - R_1][1+\xi_n]\, w_n\, w_m$$

$$\mathbf{G}^{ij} = \int_{\rho_j} \rho \left[\int_{\vartheta} \mathbf{U}_c \, d\vartheta \right] d\rho = \sum_{m=1}^{2} \sum_{n=1}^{20} (\pi/4)[(R_1 + R_2) + \eta_m(R_2 - R_1)]\mathbf{U}_c(\xi_n, \eta_m)[R_2 - R_1][1 + \xi_n] w_n w_m \tag{17}$$

where $\mathbf{T}_c(\xi_n, \eta_m)$ and $\mathbf{U}_c(\xi_n, \eta_m)$ represent the values of the matrices in equations (7) and (11) computed at the (n, m) integration point and w_n, w_m are the weights of the Gaussian quadrature formula.

When the integration is carried out over the element which contains the collocation point, a singularity exists in the fundamental solution and the integration scheme is different. First of all, the part containing the singularity is separated from the rest of the fundamental solution to be integrated. This is done by subtracting the static fundamental solution from the dynamic one. The difference is non-singular at any point of the integration domain and can be integrated by means of the same kind of numerical quadrature formula, combined with the quadratic transformation of the co-ordinate ϑ, as before.

The coefficients of equation (13) for which $i = j$ can be written as

$$\begin{aligned} \mathbf{H}^{*ii} &= \mathbf{H}^{*ii}_{\text{din}} + \mathbf{H}^{*ii}_{\text{st}} \\ \mathbf{G}^{ii} &= \mathbf{G}^{ii}_{\text{din}} + \mathbf{G}^{ii}_{\text{st}} \end{aligned} \tag{18}$$

where $\mathbf{H}^{*ii}_{\text{st}}$ and $\mathbf{G}^{ii}_{\text{st}}$ are the static counterparts of $\mathbf{H}^{*ii}$ and $\mathbf{G}^{ii}$, respectively, and

$$\begin{aligned} \mathbf{H}^{*ij}_{\text{din}} &= \int_{\rho_j} \rho \left\{ \int_{\vartheta} \left[\mathbf{T}_c - \mathbf{T}_c(\text{static}) \right] d\vartheta \right\} d\rho = \int_{\rho_j} \rho \left\{ \int_{\vartheta} \mathbf{T}_{c,\,\text{din}} \, d\vartheta \right\} d\rho \\ &= \sum_{m=1}^{2} \sum_{n=1}^{20} (\pi/4)[(R_1 + R_2) + \eta_m(R_2 - R_1)]\mathbf{T}_{c,\,\text{din}}(\xi_n, \eta_m) \\ &\quad [R_2 - R_1][1 + \xi_n] w_n w_m \\ \mathbf{G}^{ij}_{\text{din}} &= \int_{\rho_j} \rho \left\{ \int_{\vartheta} [\mathbf{U}_c - \mathbf{U}_c(\text{static})] d\vartheta \right\} d\rho = \int_{\rho_j} \rho \left\{ \int_{\vartheta} \mathbf{U}_{c,\,\text{din}} \, d\vartheta \right\} d\rho \\ &= \sum_{m=1}^{2} \sum_{n=1}^{20} (\pi/4)[(R_1 + R_2) + \eta_m(R_2 - R_1)] \\ &\quad \mathbf{U}_{c,\,\text{din}}(\xi_n, \eta_m)[R_2 - R_1][1 + \xi_n] w_n w_m \end{aligned} \tag{19}$$

where $\mathbf{T}_{c,\,\text{din}}(\xi_n, \eta_m)$ and $\mathbf{U}_{c,\,\text{din}}(\xi_n, \eta_m)$ stand for the values at ξ_n, η_m of matrices of the same form of those in equations (7) and (11) but with the difference between the dynamic and the static fundamental solution instead of the dynamic fundamental solution ($T_{kl,\,\text{din}} = T_{kl} - T_{kl}(\text{static})$ and $U_{kl,\,\text{din}} = U_{kl} - U_{kl}(\text{static})$ instead of T_{kl} and U_{kl}, respectively). Figure 6 shows the integration domains and the collocation points for this case. The process is completed with the integration of the static fundamental solution. The coefficients $T_{kl}(\text{static})$ and $U_{kl}(\text{static})$ are known in terms of the distance r and its derivatives (Figure 6):

$$\begin{aligned} r &= \sqrt{(\rho^2 + R^2 - 2R\rho\cos\vartheta)} \\ R &= \frac{R_1 + R_2}{2} \\ r_{,1} &= (R - \rho\cos\vartheta)/r \\ r_{,2} &= (\rho\sin\vartheta)/r \end{aligned} \tag{20}$$

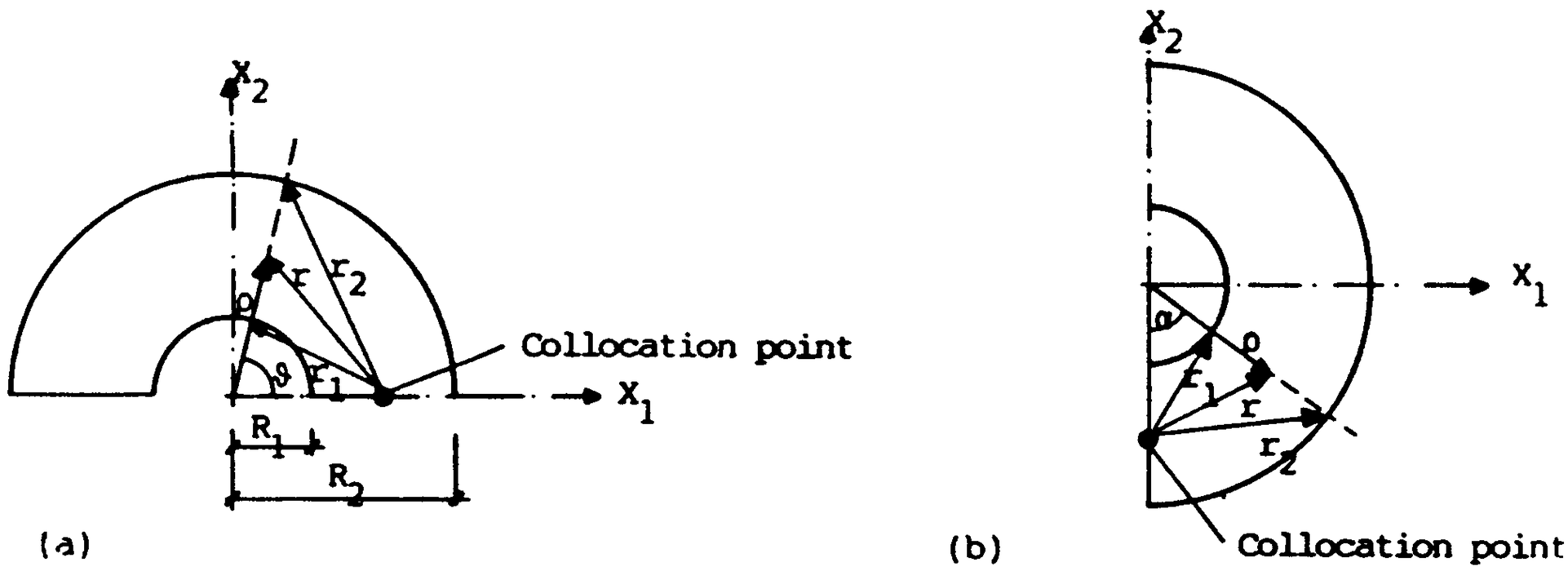

Figure 6. Integration domains and co-ordinates when the collocation point is inside the integration domain: (a) $\vartheta^i = 0$, (b) $\vartheta^i = -\pi/2$

for the case of Figure 6(a) and the same with the angle α instead of ϑ for the case of Figure 6(b). The double integrals of equations (7) and (11) may be written as an integration over ρ inside an integration over ϑ. It may easily be shown that the integration over ρ can always be reduced to a linear combination of the following integrals:

$$I_1 = \int_{R_1}^{R_2} (\rho/r)\,\mathrm{d}\rho;\; I_2 = \int_{R_1}^{R_2} (\rho/r^3)\,\mathrm{d}\rho$$

$$I_3 = \int_{R_1}^{R_2} (\rho^2/r^3)\,\mathrm{d}\rho;\; I_4 = \int_{R_1}^{R_2} (\rho^3/r^3)\,\mathrm{d}\rho \tag{21}$$

From which an exact closed form solution is easily obtained. The expressions for the double integrals of the static fundamental solution appearing in equations (7) and (11) are given in terms of I_1, I_2, I_3 and I_4 in the Appendix. After the integration over ρ has been carried out, the integration along ϑ follows the two extreme circumferences of the element. These non-singular integrals are done using the same numerical integration approach as before, i.e. a quadratic transformation of ϑ into the dimensionless variable ξ and a twenty-point Gaussian quadrature.

NUMERICAL RESULTS FOR SURFACE CIRCULAR FOUNDATION

The generalized frequency-dependent force–displacement relationship (stiffness matrix) for a massless rigid circular foundation can be written as (see Figure 7)

$$\begin{bmatrix} F_1 \\ M_1 \\ F_2 \\ M_2 \\ F_3 \\ M_3 \end{bmatrix} = \begin{bmatrix} K^*_{hh} & -K^*_{hr} & 0 & 0 & 0 & 0 \\ -K^*_{rh} & K^*_{rr} & 0 & 0 & 0 & 0 \\ 0 & 0 & K^*_{hh} & K^*_{hr} & 0 & 0 \\ 0 & 0 & K^*_{rh} & K^*_{rr} & 0 & 0 \\ 0 & 0 & 0 & 0 & K^*_{vv} & 0 \\ 0 & 0 & 0 & 0 & 0 & K^*_{tt} \end{bmatrix} \begin{bmatrix} u_1 \\ \phi_1 \\ u_2 \\ \phi_2 \\ u_3 \\ \phi_3 \end{bmatrix} \tag{22}$$

The stiffness functions are written as

$$K^*_{ij} = K_{ij}(k_{ij} + i a_0 c_{ij}),\ (i,j = \mathrm{h},\ \mathrm{r},\ \mathrm{v},\ \mathrm{t}) \tag{23}$$

where K_{ij} is the static value, k_{ij} and c_{ij} are the dynamic stiffness and damping coefficients, respectively, and $a_0 = \omega R/C_s$ is the dimensionless frequency. R is the foundation radius and C_s the shear-wave velocity of the material under the foundation. Each material is defined by a complex modulus $G^* = G(1+2i\xi)$ in which ξ is the material damping; ρ is the density and v is Poisson's ratio. Each column of the stiffness matrix is obtained prescribing a unit displacement or rotation following one of the co-ordinates and computing the resultant force and moment at the foundation centre point.

Foundation on a uniform half-space

A first test of the proposed approach is obtained by the comparison of the calculated dynamic stiffness and damping coefficients, of a circular foundation on a half-space, with analytical solutions obtained assuming relaxed contact conditions.[1,2] The material is assumed to be perfectly elastic with a Poisson's ratio $v = 1/3$. Welded contact conditions between the soil and the foundation are used in the present study. The boundary element discretization under the foundation consists of eight constant elements of variable length (Figure 8). Even though a complete space fundamental solution is used, the soil free surface is not discretized because the effect of those elements on the foundation stiffness would be very small. In fact if 'smooth' contact between the foundation and the soil were assumed the free-surface element would not have any effect at all on the equations of the interface elements.[6]

Figure 9 shows a comparison between the stiffness coefficients computed by the proposed approach and the analytical solutions published by Veletsos and Wei[1] and by Luco and Westmann.[2] The agreement between the results can be considered as good, in particular when the simplicity of the mesh (only eight constant elements) and the kind of contact conditions used in

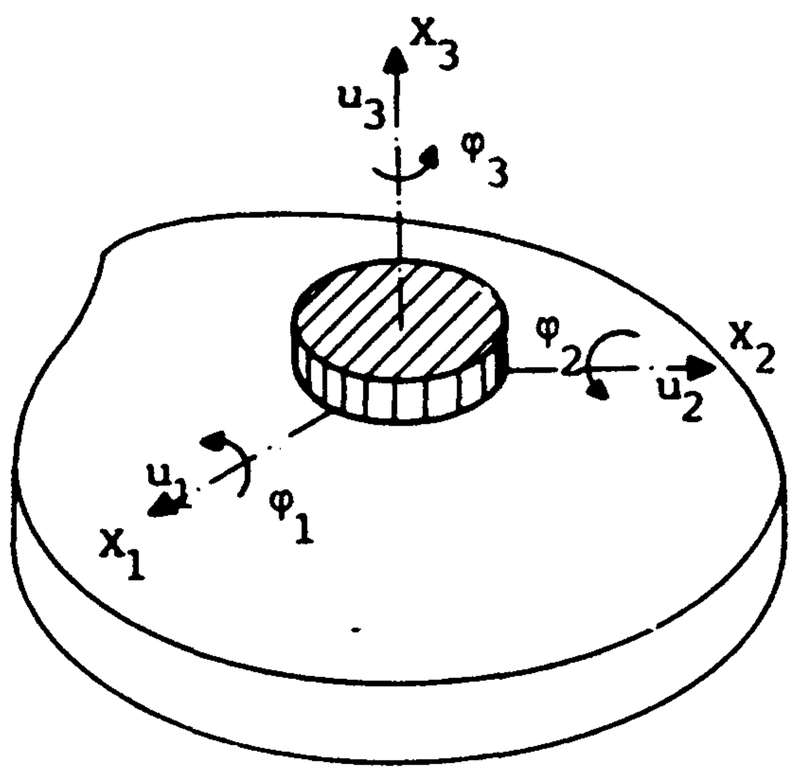

Figure 7. Description of model and co-ordinate system

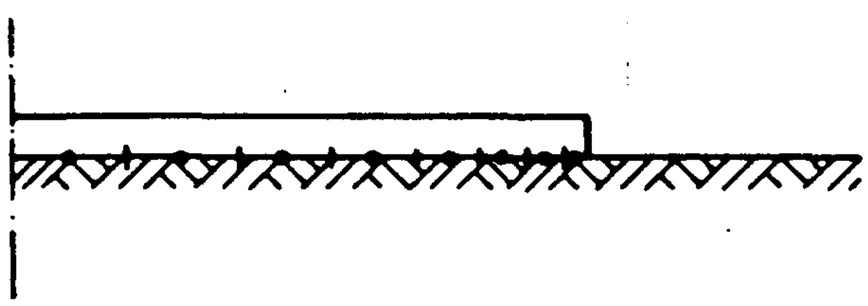

Figure 8. Boundary discretization for circular foundation on a half-space

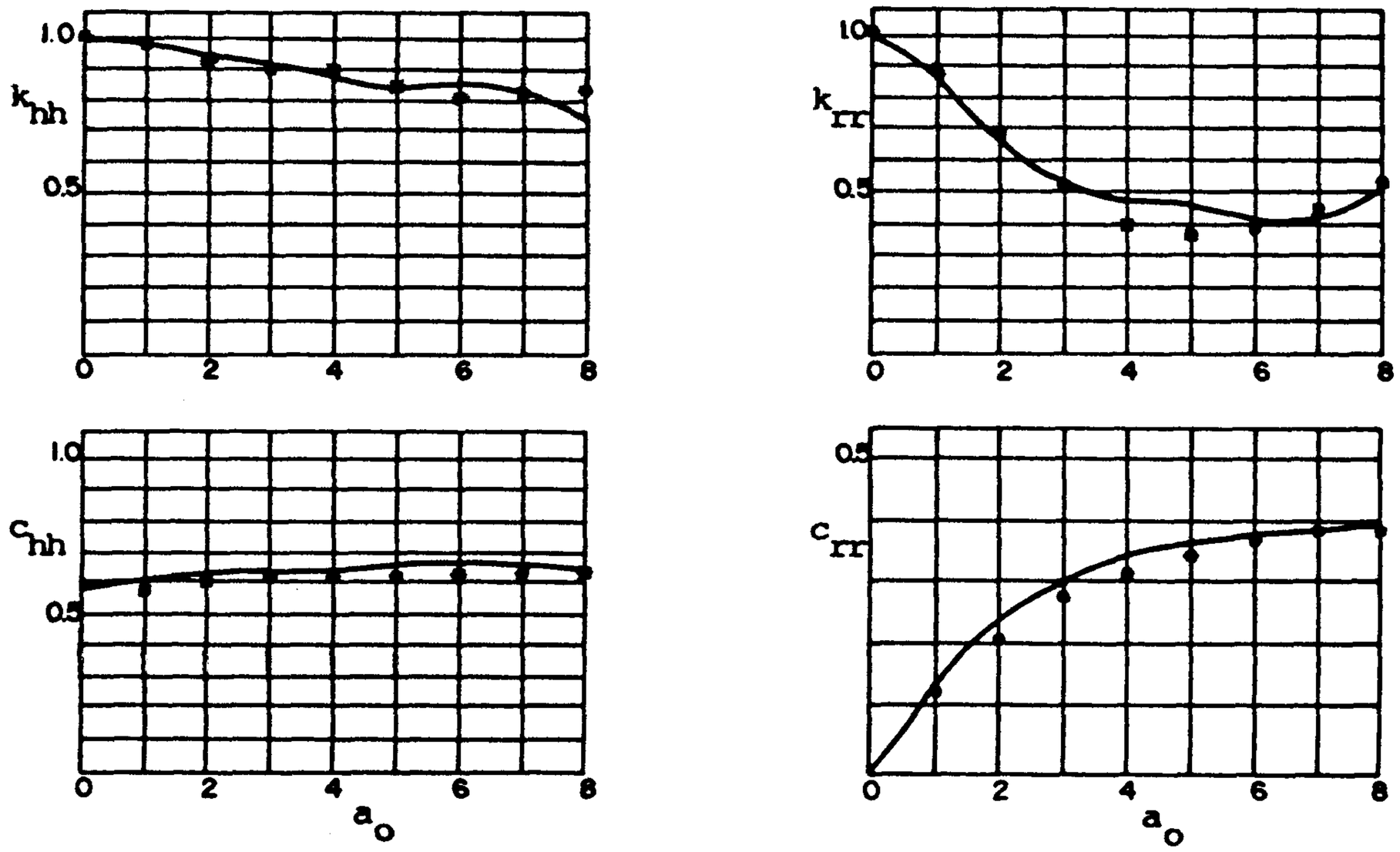

Figure 9. Stiffness coefficients for circular foundation on an elastic half-space ($\nu = 1/3$)

each study are taken into account. A zero damping factor has been considered for the half-space. This perfectly elastic material cannot be modelled by some other numerical approaches which have to include a certain amount of material damping. Results for values of a_0 as low as 0·01 have been obtained without any numerical difficulty. Results for $a_0 = 0$ have also been computed.

To complete the half-space study, a viscoelastic half-space with a damping factor $\xi = 0{\cdot}15$ is analysed. Results computed using the proposed approach with the eight-element discretization of Figure 8 are shown in Figure 10. Results obtained by Luco[21, 23] by numerical solution of sets of integral equations and using relaxed contact conditions for horizontal, vertical and rocking stiffness coefficients are also shown for comparison. The agreement is very good.

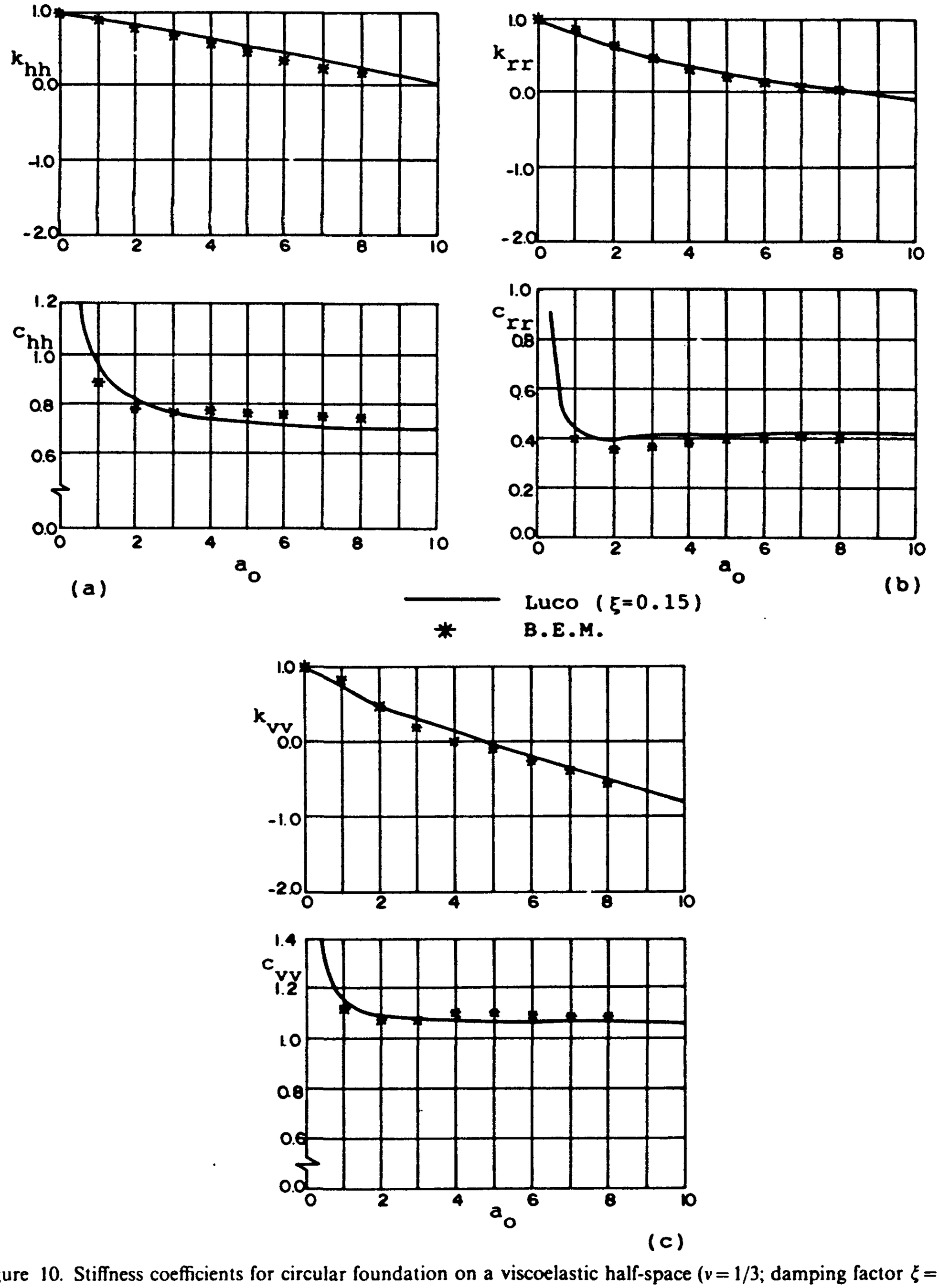

Figure 10. Stiffness coefficients for circular foundation on a viscoelastic half-space ($\nu = 1/3$; damping factor $\xi = 0{\cdot}15$)

Foundation on a soil layer on a half-space

The following example has been chosen to test the capability of the proposed approach to compute dynamic stiffness coefficients in cases where there are resonance peaks due to the existence of a soil layer on a stiffer bedrock. The results are compared with those obtained by Chapel[19] using a boundary element approach and with the results presented by Luco.[22] The same properties of References 19 and 22 have been assumed. The soil layer is characterized by Young's modulus $E_1 = 1{\cdot}76 \times 10^6$ N/m^2, Poisson's ratio $\nu_1 = 0{\cdot}3$ and density $\rho_1 = 1{\cdot}7 \times 10^3$ kg/m^3. The uniform half-space is characterized by Young's modulus $E_2 = 1{\cdot}25 \times 10^7$ N/m^2, Poisson's ratio $\nu_2 = 0{\cdot}25$ and density $\rho_2 = 2 \times 10^3$ kg/m^3. The above properties lead to a shear-wave velocity ratio $RC_s = C_{s2}/C_{s1} = 2{\cdot}5$. Two different layer depths are analysed: $H/R = 0{\cdot}5$ and $H/R = 1$.

Figure 11 shows the model and the boundary element discretization. The soil–foundation interface has the same element distribution as the previous example. Seven elements have been placed on the soil free surface, their length being $R/4$ for the first two and $R/2$ for the other five. The interface between the two materials has been discretized into eight elements with a length equal to $R/2$.

The values of the computed vertical stiffness coefficients normalized by the static stiffness of a uniform half-space with the properties of the soil layer are shown in Figure 12 for a frequency range $0 \leq a_0 \leq 6$ and two layer depths. The results obtained by Chapel[19] and Luco[22] for the same problems are also represented. The calculated values agree very well with Luco's. The results of Chapel are, in general, in good correlation with the other two; however, they show more differences with the computed and Luco's results than those existing between the latter two.

Foundation on a multilayered soil on a half-space

The last example corresponds to a layered soil based on a half space. The problem is the same as that studied by Luco in Reference 21 using an approach based on numerical solution of sets of integral equations. The depth of the upper boundary of each region and the material properties are given in Table I. The foundation radius is 52·5 feet.

The discretization of the boundaries is done automatically in the code according to the following criteria: (1) the soil–foundation interface is discretized into the same eight elements as the two previous examples; (2) a soil free surface equal to three times the radius is discretized; (3) the length of the free-surface elements is equal to the minimum of two values; one half of the minimum S-wavelength of a layer and the minimum layer thickness, except for the two elements closest to the foundation, the lengths of which are set equal to $R/4$; (4) the discretization of the interfaces between layers is the same as that of the soil free surface except for the three elements closest to the axis, the lengths of which are set equal to $R/2$. These criteria, that give rise to the discretization

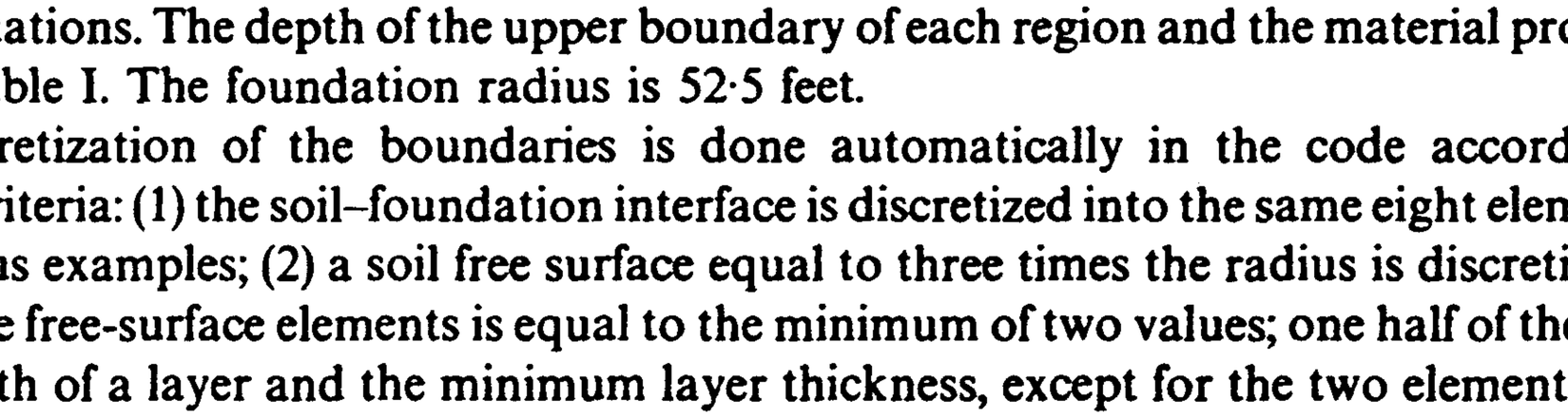

Figure 11. Circular foundation on a soil layer on a half space. Model and boundary element discretization

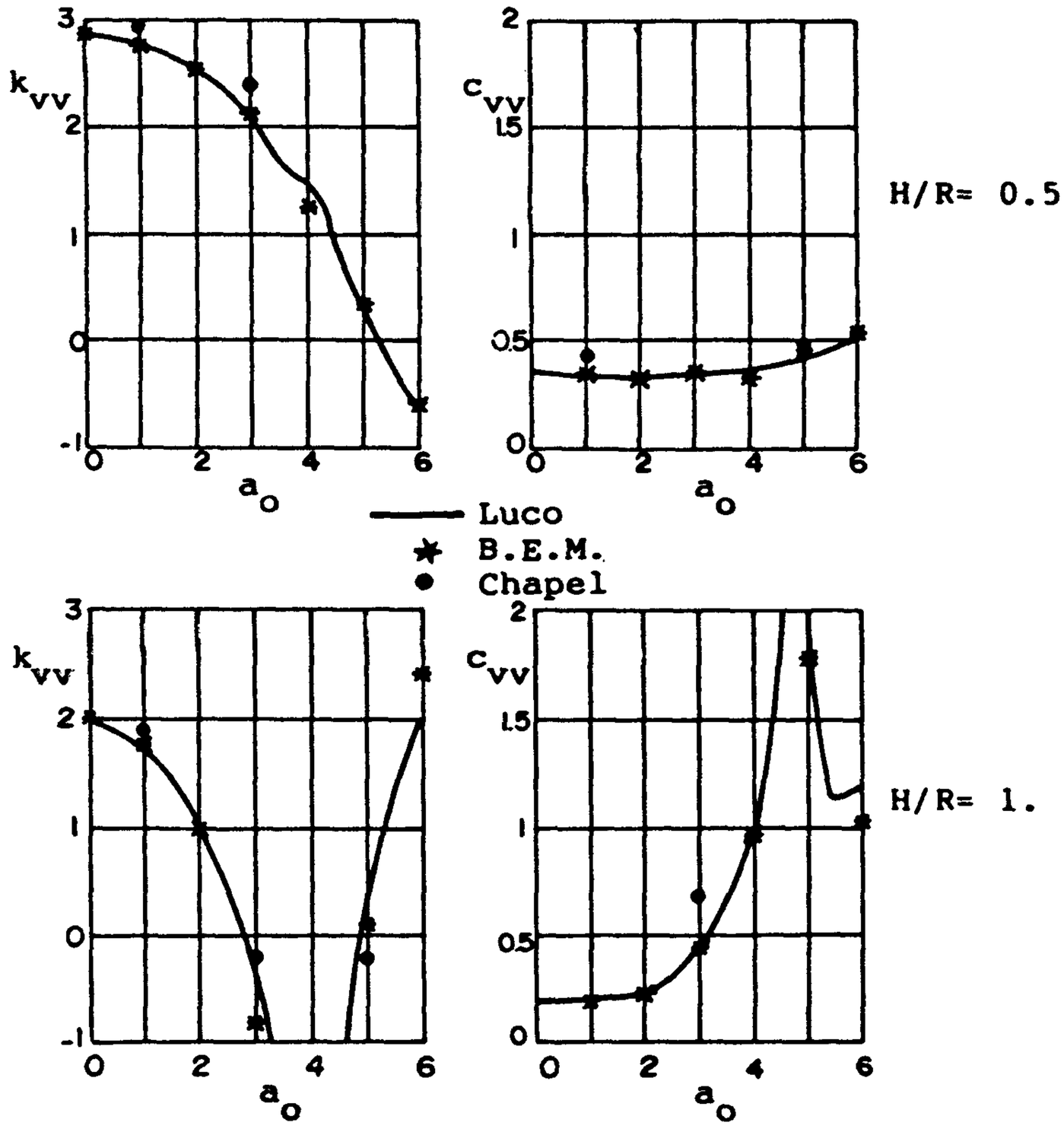

Figure 12. Vertical stiffness coefficients for circular foundation on a soil layer on a half space

Table I. Depth and properties of the soil layers and the half-space (foundation radius = 52·5 feet)

Layer	S-wave velocity C_s	Density ρ	Poisson's ratio ν	Damping factor ξ	Depth of the upper boundary
1	3004	143	0·36	0·03	0
2	2198	138	0·37	0·05	49·2
3	3333	160	0·35	0·03	114·8
4	1703	136	0·37	0·07	213·2
Half-space	2522	150	0·39	0·06	377·2

Units are: pounds, feet and seconds

shown in Figure 13 for the range of frequencies under study, were applied to the previous example as well. Comparisons of the normalized stiffness and damping coefficients obtained by the present approach with the results of Luco are presented in Figure 14 for dimensionless frequencies in the range from 0 to 1·4. The stiffness coefficients have been normalized using the static stiffness of a uniform half-space with the properties of the upper layer. The shear-wave velocity of the upper layer is used to normalize the frequency. In general, the agreement of the results shown in Figure 14 is good. The differences shown in the Figure can be explained to some extent by the different kinds of contact conditions used by the authors and by Luco.

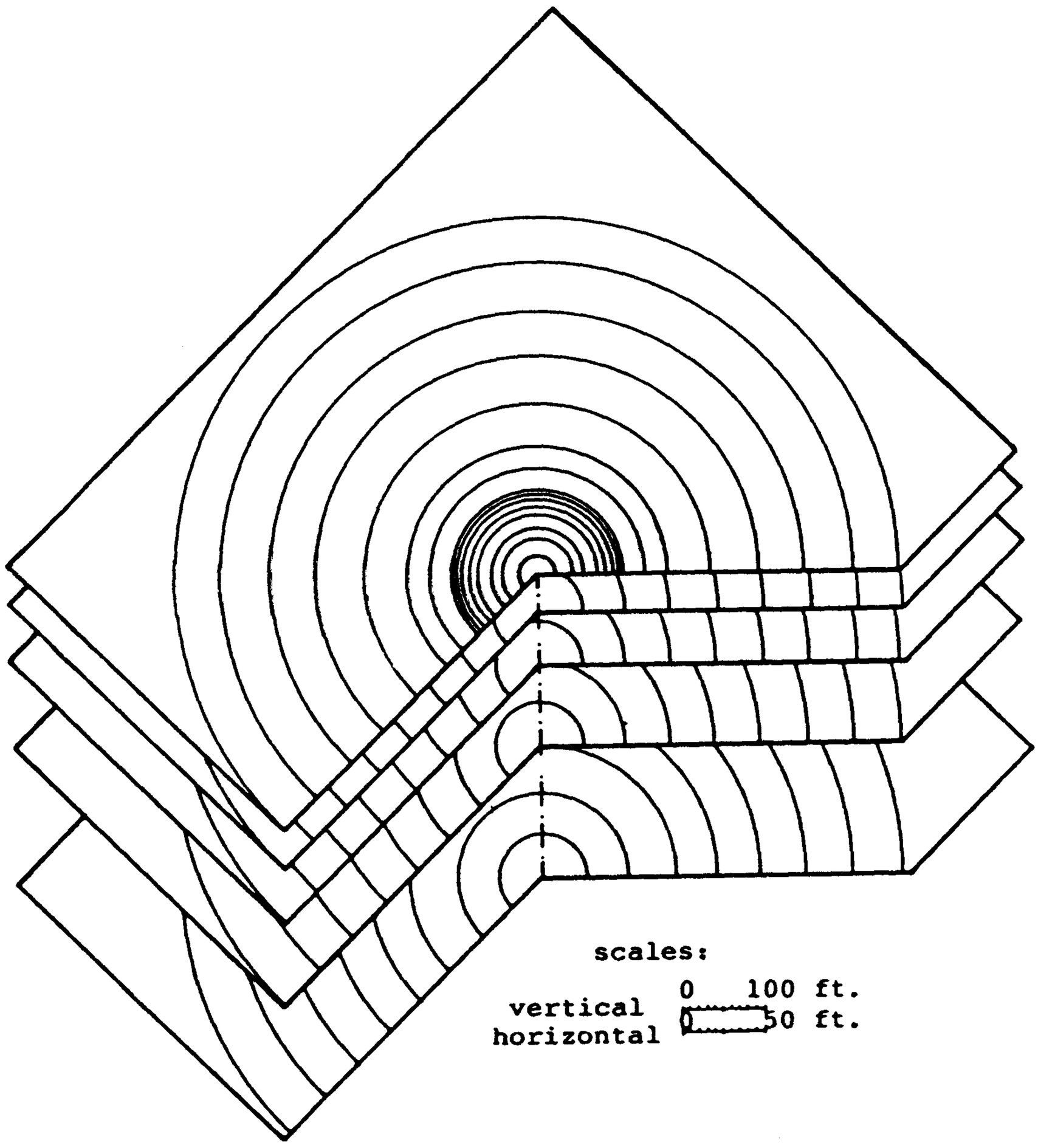

Figure 13. Circular foundation on a multilayered soil on a half-space. Boundary element discretization

CONCLUSIONS

Dynamic stiffness functions of rigid circular foundations on a uniform or layered viscoelastic soil have been computed by a boundary element approach that makes use of the complete space point load fundamental solution. This solution is simple and easy to integrate over the boundary elements. The price paid for using such a simple fundamental solution is that the soil free surface and the layer interfaces have to be discretized. However, the discretization of the soil surface and the layer interfaces can be reduced to a limited zone sorrounding the foundation and is automatically done by the code.

Approaches based on Green's functions for a layered half-space[7,9-11] have the advantage of requiring only the discretization of the soil foundation interface but have the disadvantage of dealing with a fundamental solution that is not known in closed form but in terms of integral forms that include products of two Bessel functions and have to be evaluated segmentally by elaborated numerical integration procedures. The proposed approach is easier to implement than those other

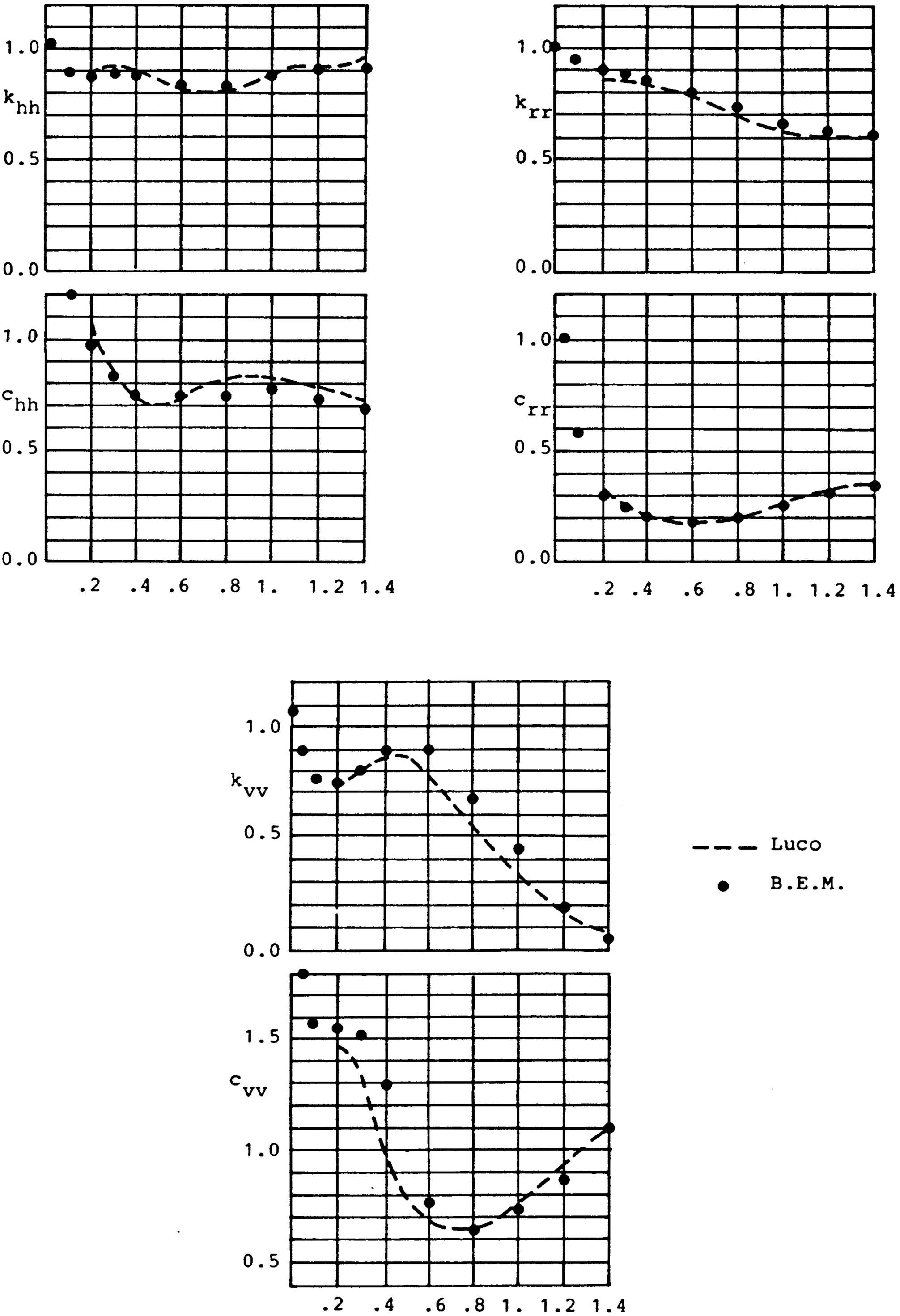

Figure 14. Stiffness coefficients for circular foundation on a multilayered soil on a half space

approaches. The amount of computer time required to solve a particular problem is smaller for one case or the other depending on the number of layers in the soil profile.

To illustrate the capabilities of the proposed approach, dynamic stiffness functions for a uniform half-space and two layered soils have been obtained. The results obtained for the half-space have been validated by comparison with analytical solutions; those for the layered soils by comparison with the results of an approach based on numerical solution of sets of integral equations and, in the case of a single soil layer on a half-space, also by comparison with other boundary element results. The comparisons indicate a good degree of accuracy.

ACKNOWLEDGEMENTS

The work described herein is partially supported by a grant provided by the local government of Andalusia, Spain. The authors express their sincere appreciation for this support.

APPENDIX

Integrals of the static part of the fundamental solution over the element where the point load is located, are given in this Appendix.

Terms corresponding to vertical or torsional motion of the foundation (equation (7)):

$$G^{ii}_{11c,st} = 2\int_{\rho_i}\int_0^{\pi} U_{11c,st}\,\rho\,d\vartheta\,d\rho$$

$$= 2A\int_{\rho_1}\int_0^{\pi}\left[\frac{B\cos\vartheta}{r}+\frac{\rho^2}{r^3}\cos\vartheta+\frac{R^2}{r^3}\cos\vartheta-\frac{\rho R}{r^3}(1+\cos^2\vartheta)\right]\rho\,d\vartheta\,d\rho$$

$$= 2A\left[B\int_0^{\pi} I_1\cos\vartheta\,d\vartheta+\int_0^{\pi} I_4\cos\vartheta\,d\vartheta+R^2\int_0^{\pi} I_2\cos\vartheta\,d\vartheta\right.$$

$$\left.-R\int_0^{\pi} I_3(1+\cos^2\vartheta)\,d\vartheta\right] \tag{24}$$

where $A=(1/16)\pi\mu(1-\nu)$ and $B=3-4\nu$.

$$G^{ii}_{22c,st}=2\int_{\rho_i}\int_0^{\pi} U_{22c,st}\,\rho\,d\vartheta\,d\rho = 2A\int_{\rho_i}\int_0^{\pi}\left[\frac{B\cos\vartheta}{r}+\frac{\rho R\sin^2\vartheta}{r^3}\right]\rho\,d\vartheta\,d\rho$$

$$= 2A\left[B\int_0^{\pi} I_1\cos\vartheta\,d\vartheta+R\int_0^{\pi} I_3\sin^2\vartheta\,d\vartheta\right] \tag{25}$$

$$G^{ii}_{33c,st}=2\int_{\rho_i}\int_0^{\pi} U_{33c,st}\,\rho\,d\vartheta\,d\rho = 2A\int_{\rho_i}\int_0^{\pi}\frac{B}{r}\rho\,d\vartheta\,d\rho = 2AB\int_0^{\pi} I_1\,d\vartheta \tag{26}$$

$$G^{ii}_{12c,st}=G^{ii}_{13c,st}=G^{ii}_{23c,st}=G^{ii}_{21c,st}=G^{ii}_{31c,st}=G^{ii}_{32c,st}=0 \tag{27}$$

$$H^{*ii}_{13c,st}=2\int_{\rho_i}\int_0^{\pi} T_{13c,st}\,\rho\,d\vartheta\,d\rho = 2A\int_{\rho_i}\int_0^{\pi}\left[\frac{B}{r^3}(\rho\cos\vartheta-R)\right]\rho\,d\vartheta\,d\rho$$

$$= 2AB\left[\int_0^{\pi} I_3\cos\vartheta\,d\vartheta-R\int_0^{\pi} I_2\,d\vartheta\right] \tag{28}$$

$$H^{*ii}_{31c,st} = 2\int_{\rho_i}\int_0^{\pi} T_{31c,st}\,\rho\,d\vartheta\,d\rho = 2A\int_{\rho_i}\int_0^{\pi}\left[\frac{-B}{r^3}(\rho - R\cos\vartheta)\right]\rho\,d\vartheta\,d\rho$$

$$= -2AB\left[\int_0^{\pi} I_3\,d\vartheta - R\int_0^{\pi} I_2\cos\vartheta\,d\vartheta\right] \tag{29}$$

$$H^{*ii}_{11c,st} = H^{*ii}_{22c,st} = H^{*ii}_{33c,st} = H^{*ii}_{12c,st} = H^{*ii}_{21c,st} = H^{*ii}_{23c,st} = H^{*ii}_{32c,st} = 0 \tag{30}$$

Terms corresponding to horizontal or rocking motion (equation (11)):

$$G^{ii}_{11c,st} = 2A\left[B\int_0^{\pi} I_1\cos^2\vartheta\,d\vartheta + \int_0^{\pi} I_4\cos^2\vartheta\,d\vartheta\right.$$

$$\left. + R^2\int_0^{\pi} I_2\cos^2\vartheta - R\int_0^{\pi} I_3(1+\cos^2\vartheta)\cos\vartheta\,d\vartheta\right. \tag{31}$$

$$G^{ii}_{12c,st} = 2A\left[B\int_0^{\pi} I_1\sin^2\vartheta\,d\vartheta + R^2\int_0^{\pi} I_2\sin^2\vartheta\,d\vartheta - R\int_0^{\pi} I_3\sin^2\vartheta\cos\vartheta\,d\vartheta\right] \tag{32}$$

$$G^{ii}_{22c,st} = 2A\left[B\int_0^{\pi} I_1\cos^2\alpha\,d\alpha + R\int_0^{\pi} I_3\sin^2\alpha\cos\alpha\,d\alpha\right] \tag{33}$$

$$G^{ii}_{21c,st} = 2A\left[B\int_0^{\pi} I_1\sin^2\alpha\,d\alpha + \int_0^{\pi} I_4\sin^2\alpha\,d\alpha - R\int_0^{\pi} I_3\sin^2\alpha\cos\alpha\,d\alpha\right] \tag{34}$$

$$G^{ii}_{33c,st} = 2AB\int_0^{\pi} I_1\cos\vartheta\,d\vartheta \tag{35}$$

$$G^{ii}_{13c,st} = G^{ii}_{23c,st} = G^{ii}_{31c,st} = G^{ii}_{32c,st} = 0 \tag{36}$$

$$H^{*ii}_{13c,st} = 2AB\left[\int_0^{\pi} I_3\cos^2\vartheta\,d\vartheta - R\int_0^{\pi} I_2\cos\vartheta\,d\vartheta\right] \tag{37}$$

$$H^{*ii}_{23c,st} = 2AB\int_0^{\pi} I_3\sin^2\vartheta\,d\vartheta \tag{38}$$

$$H^{*ii}_{31c,st} = -2AB\left[\int_0^{\pi} I_3\cos\vartheta\,d\vartheta - R\int_0^{\pi} I_2\cos^2\vartheta\,d\vartheta\right] \tag{39}$$

$$H^{*ii}_{32c,st} = 2ABR\int_0^{\pi} I_2\sin^2\vartheta\,d\vartheta \tag{40}$$

$$H^{*ii}_{11c,st} = H^{*ii}_{22c,st} = H^{*ii}_{33c,st} = H^{*ii}_{12c,st} = H^{*ii}_{21c,st} = 0 \tag{41}$$